# A new convective adjustment scheme.
# Part II: Single column tests using GATE wave, BOMEX, ATEX and arctic air-mass data sets

By A. K. BETTS*
*West Pawlet, VT 05775, U.S.A.*

and

M. J. MILLER
*ECMWF, Reading*

SUMMARY

The schemes proposed in part I are tested using single-column data sets from tropical field experiments (GATE, BOMEX, ATEX) and an arctic air-mass transformation. Both the deep and shallow schemes perform well. The sensitivity of the schemes to adjustable parameters is also studied. Preliminary global forecasts show significant improvements in the global surface fluxes and mean tropical temperature tendency over the operational Kuo convection scheme.

## 1. INTRODUCTION

The convective parametrization scheme described in part I (Betts 1986) was tested and tuned using a series of single-column data sets from field experiments. A GATE wave data set (derived from Thompson *et al.* 1979) was used to test and develop the deep convection scheme. BOMEX (from Holland and Rasmusson 1973) and ATEX (from Augstein *et al.* 1973 and Wagner 1975) data sets were used to test and develop the shallow convection scheme. A fourth data set for an arctic air-mass transformation (from Økland 1976) was used to test both schemes with strong surface fluxes. This is a companion paper to Betts (1986), where the symbols and equations are presented.

## 2. DEEP CONVECTION

### (a) GATE wave data set

The ECMWF grid-point model was run as a single column model with prescribed GATE phase III radiation (from Cox and Griffith 1979) and prescribed heat and moisture tendencies due to adiabatic processes (from Thompson *et al.* 1979). The adiabatic forcing terms have a wave structure with 80 h period. The model was integrated in time from an initial sounding using the convection scheme. The temperature and moisture structure, the precipitation and the vertical profile of the convective heating and drying terms as a function of time can be compared with those diagnosed from observations. Most of the sensitivity tests were done with surface fluxes prescribed as well (from Thompson *et al.* 1979), using an 18-level single-column version of the European Centre's model. (The cloud base level was specified as the lowest model level (about 982 mb).) Section 2(*d*) will show results with an extra level below the cloud layer and an interactive boundary layer scheme.

### (b) Optimum parameter set

We shall present first an optimum parameter set (Table 1) to show how well the scheme can reproduce the structure of the mean GATE wave. Section 2(*c*) shows how these parameters were selected using sensitivity tests.

* Visiting Scientist, ECMWF.

TABLE 1. CONVECTION SCHEME OPTIMUM PARAMETERS. EQUATION NUMBERS ARE FROM PART I

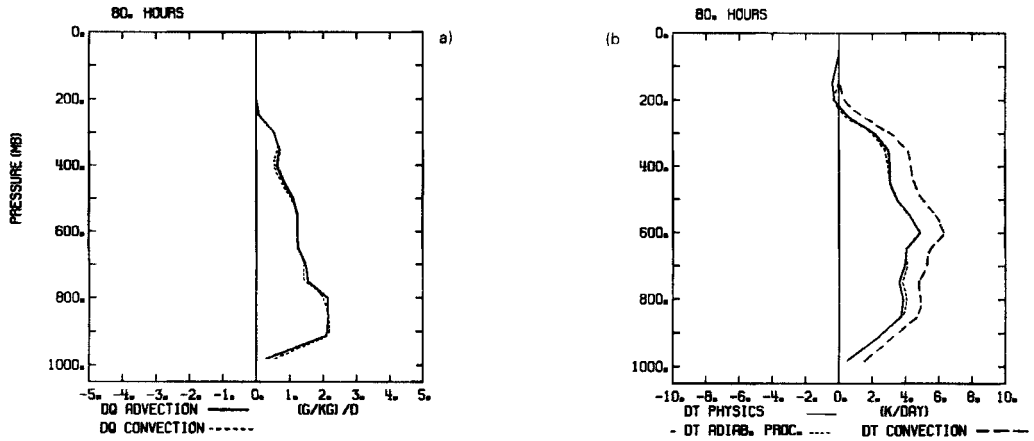| Adjustment time (Eq. (4)) | Stability parameter (Eq. (15)) | Subsaturation parameters (mb) (Eqs. (17), (18)) | | |
|---|---|---|---|---|
| | | Cloud base $\mathscr{P}_B$ | Freezing level $\mathscr{P}_M$ | Cloud top $\mathscr{P}_T$ |
| $\tau$ (hours) | $\alpha$ | | | |
| 2 | 1·5 | −25 | −50 | −38 |



Figure 1. 80-hour mean vertical structure of prescribed adiabatic forcing terms and parametrized drying and heating for GATE wave data due to convection and surface fluxes.

Figures 1(a, b) show the 80-hour mean vertical structure of the moisture and heat budgets; (a) shows the prescribed moisture advection and the convective response, and (b) the prescribed adiabatic forcing term, the convective heating and the model 'physics' (convective scheme, plus prescribed radiation and surface fluxes). The mean balance is very precise, although the lower troposphere cools and the upper troposphere warms slightly. Figures 2(a, b) show temperature and dew-point for the computed 40 h and 80 h sounding compared with the observations showing the same result. At 40 h (the wave trough) the agreement between model scheme and the observed mean structure is very
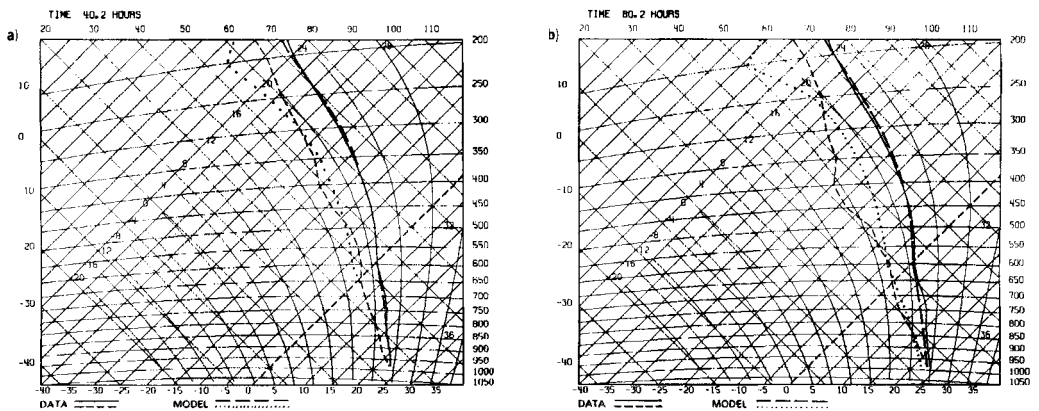


Figure 2. Comparison of observed sounding ($T$, $T_D$) and computed sounding: (a) 40 hours (trough); and (b) 80 hours (ridge).
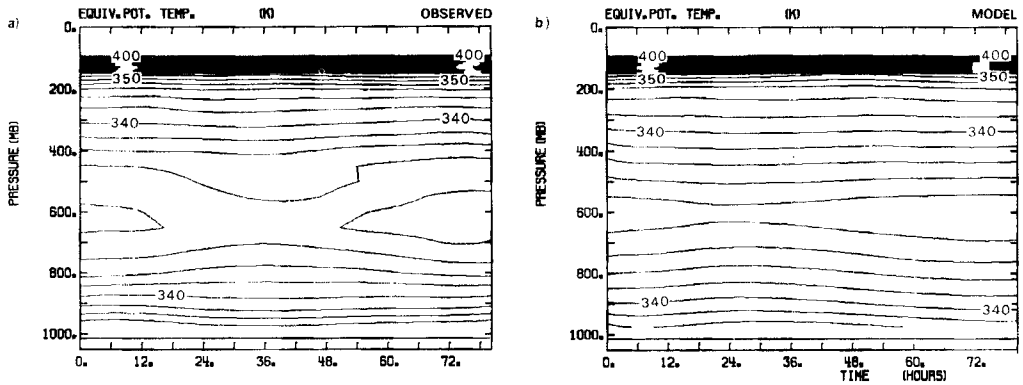
Figure 3.   Comparison of (a), observed and (b), computed $\theta_E$ structure of GATE wave.
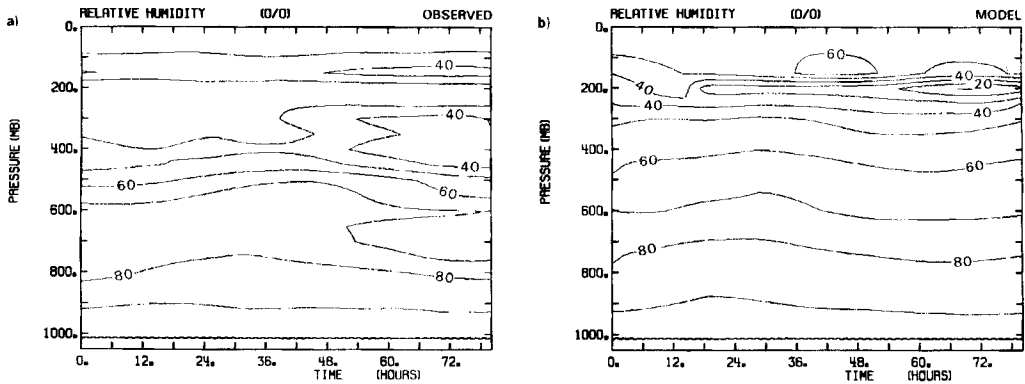


Figure 4.   Comparison of (a), observed and (b), computed relative humidity for GATE wave.

good, although the convection scheme does not reproduce the subsequent drying out of the upper troposphere at the ridge (80 h).

Figures 3, 4, 5 compare the time–height cross-sections for the data (observed structure and diagnosed convective source terms) with those predicted by the model using the convection scheme. Figure 3 shows the evolution of the wave in equivalent potential temperature for (a), observations and (b), model prediction using the convection scheme. The agreement is good, although as in Fig. 2, the observations are warmer and moister at the lowest level. Figure 4 shows the same comparison for relative humidity, showing fairly good agreement. The convection scheme does not maintain relative humidity well at 200 mb, near cloud top. Figures 5 and 6 compare diagnosed and computed convective heat source and moisture sink (plus surface fluxes), showing how well the parametrization scheme reproduces the general wave structure of the convective source terms with their maxima at different pressure levels. The agreement is excellent.

Figure 7 compares the observed rainfall with that computed by the model. We see good agreement in amplitude but not in phase. The convection scheme, which is closely coupled to the moisture advection, cannot reproduce the observed lag of the precipitation which appears to be due to subgrid-scale storage of moisture presumably in the cloud fields (Betts 1978; Frank 1978).

In general the parametrization scheme does well in reproducing the structure of the convective source terms and the precipitation. In its present form it does not reproduce
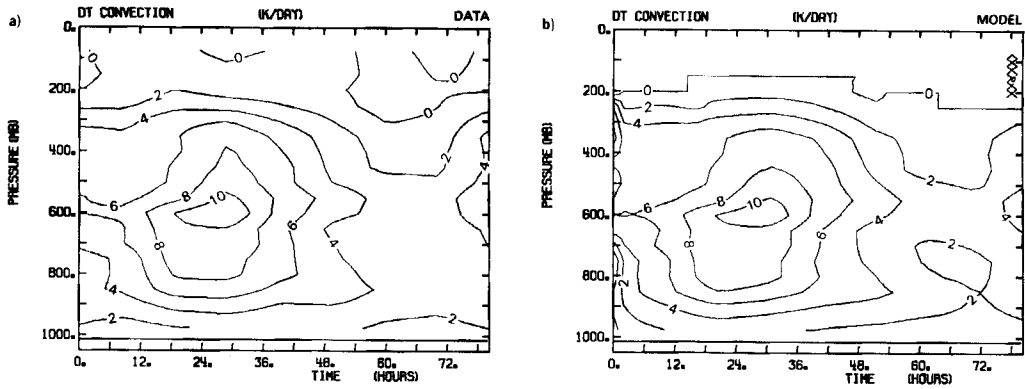
Figure 5.   Comparison of (a), diagnosed and (b), computed convective heating for GATE wave data.
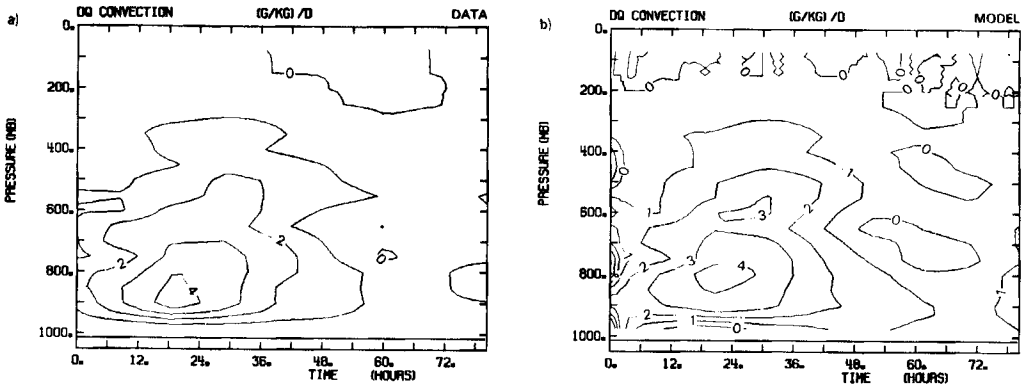


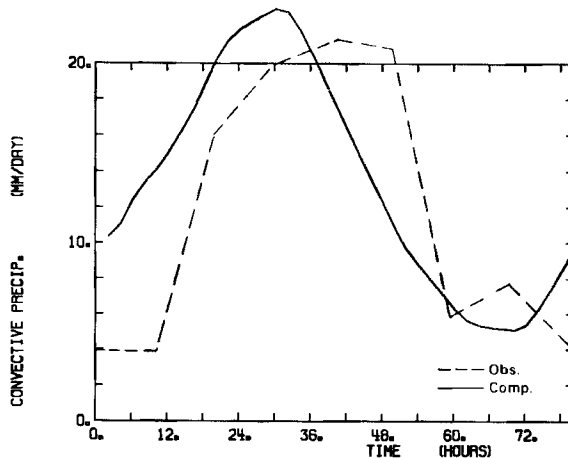Figure 6.   As Fig. 5, for convective drying.



Figure 7.   Comparison of observed and computed rainfall.

subgrid-scale moisture storage. The deficiencies in the low-level structure seen in Fig. 2 can be markedly reduced using an improved resolution and an interactive surface boundary layer (see section 4). Some deficiencies near cloud top are always likely because the adjustments at this level are always sensitive to the exact specification of cloud top

height in terms of the limited model vertical resolution. Further tuning may be possible. The GATE tests were first run with a cloud top interpolated between model levels in the specification of the adjustment profile (Eq. (16), Betts 1986). However, this proved to be an unnecessary complication and was dropped from the scheme for the subsequent interactive (section 2(d)) boundary layer test and global model tests. In sections 2(b) and 2(c) we have retained the interpolated cloud top because a few of the results, although substantially the same, are smoother (cloud top does not jump between levels) and are therefore easier to compare.

### (c) Sensitivity tests

The parameters used in 2(b) were selected after running a series of sensitivity tests. One of the advantages of this adjustment scheme is that its parameters are readily tuned separately by comparison with an observational data set. Our basic parameters will be $\tau = 2$ hours, $\mathscr{P} = -30$ mb (independent of height) and $\alpha = 1.0$. Each will be varied separately, while keeping the others constant.

(i) *Changing adjustment time scale* $\tau$. The adjustment time scale determines the lag of the convective response to large-scale forcing. With small $\tau$ the model adjusts rapidly towards the specified thermodynamic profile, while with larger $\tau$, the model atmosphere moves in the direction of the large-scale forcing. Figure 8 shows the wave in relative humidity (r.h.) for $\tau = 1, 2, 3, 5$ h ($\mathscr{P} = -30$ mb, $\alpha = 1.0$). For small $\tau$, the wave nearly disappears, while for any larger $\tau$ (>5 h), the atmosphere saturates in the wave trough
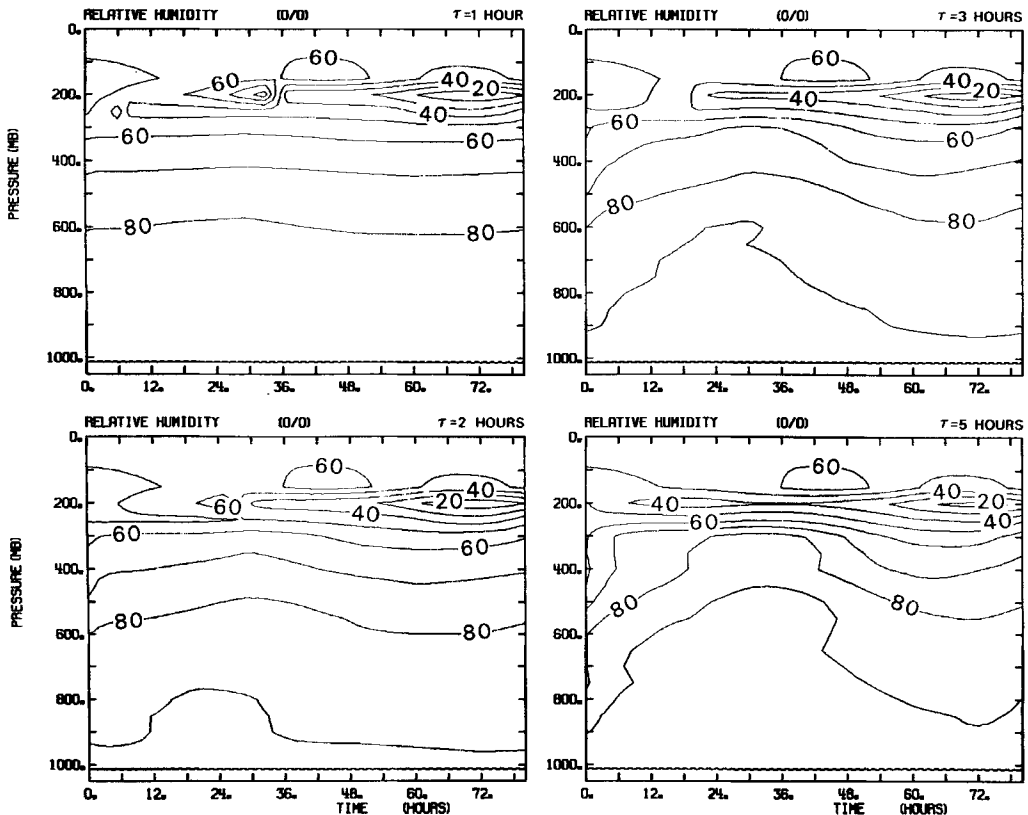


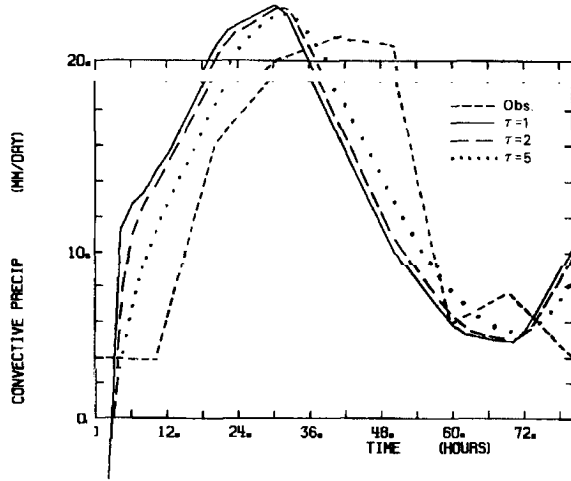Figure 8. Relative humidity wave for adjustment time scales $\tau = 1, 2, 3, 5$ hours.

Figure 9. Precipitation curves for $\tau = 1$, 2 and 5 hours compared with observed precipitation

where the large-scale forcing is large. $\tau \sim 2\,\text{h}$ gives a wave amplitude in r.h. similar to that observed (see Fig. 4). Some parameters such as the overall precipitation and the vertical temperature structure are affected rather little by changing $\tau$. The phase of the precipitation is shifted (Fig. 9) as $\tau$ increases, but even for $\tau = 5\,\text{h}$ (which gives an
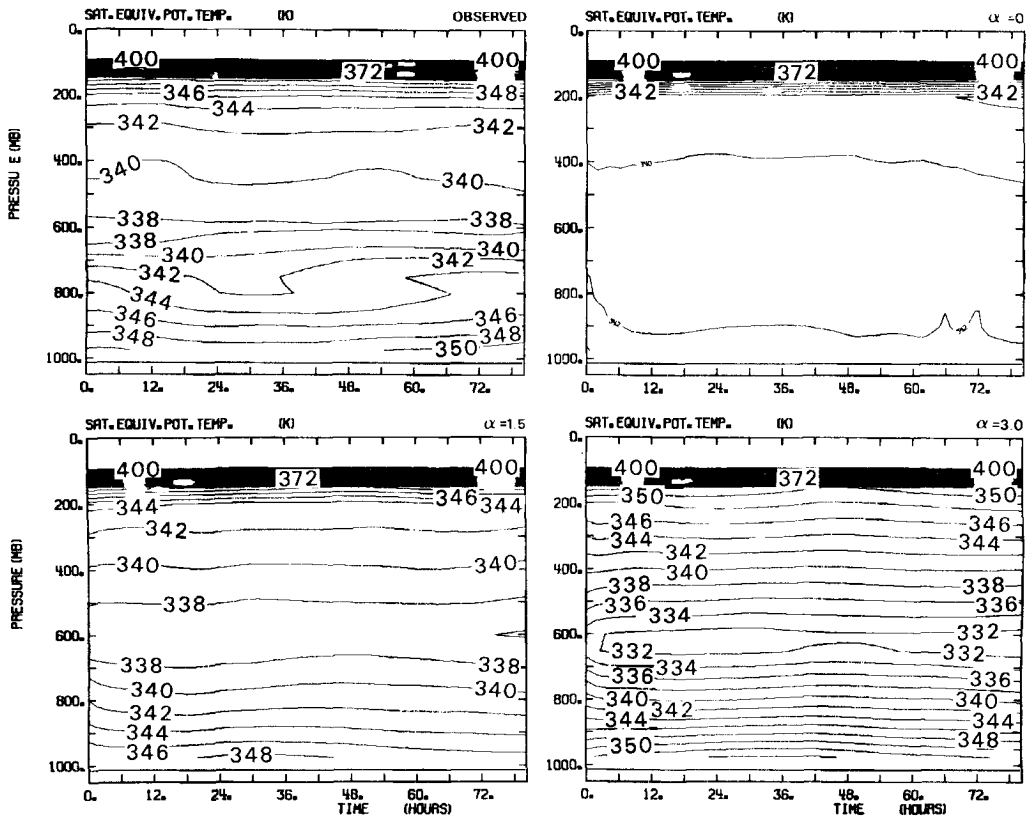


Figure 10. Comparison of observed $\theta_{ES}$ structure of wave with model structure for stability parameter $\alpha = 1.5$, 0 and 3.

unrealistic wave in relative humidity) the model precipitation is ahead of that observed. As mentioned in section 2(*b*), this is because the adjustment scheme does not allow for subgrid-scale storage of water, which appears to be responsible for the lag of precipitation behind moisture convergence in the GATE data (Betts 1978; Frank 1978).

(ii) *Changing the instability parameter* $\alpha$. The parameter $\alpha$ (Eq.(15) in part I) determines the slope of the temperature profile in relation to the $\theta_{ESV}$ isopleth, and hence the mid-tropospheric $\theta_{ES}$ minimum. This slope is easy to compare with observational data. Figure 10 shows the comparison of the $\theta_{ES}$ structure for the data: $\alpha = 1 \cdot 5$ (which is a good fit); $\alpha = 0 \cdot 0$ (almost a moist adiabat); and $\alpha = 3 \cdot 0$ (which is very unstable in the low troposphere).
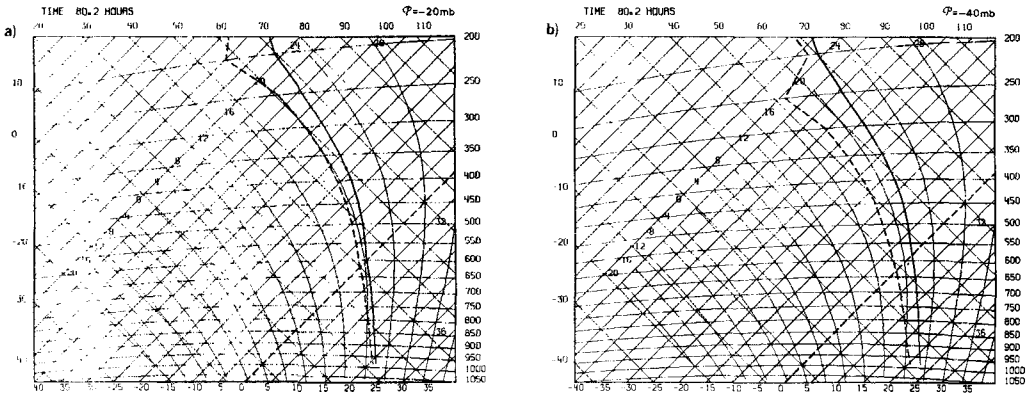


Figure 11.  Model thermodynamic structure at 80 h for the subsaturation parameter: (a) $\mathscr{P} = -20$ mb; (b) $\mathscr{P} = -40$ mb ($\alpha = 1$, $\tau = 2$ h).

(iii) *Changing saturation pressure departure* $\mathscr{P}$. $\mathscr{P}$ is closely related to subsaturation, so changing $\mathscr{P}$ alters the equilibrium relative humidity. It does not change the $\theta_E$ structure significantly, so that the lower troposphere becomes warmer and dries as $\mathscr{P}$ increases. The changes in the upper troposphere are much smaller. Figures 11(a,b) show the sounding structure at 80 h for $\mathscr{P} = -20$ and $-40$ mb illustrating this. For $\mathscr{P} = -10$ mb the atmosphere saturates during the wave passage. Figure 12 shows the computed precipitation for $\mathscr{P} = -20, -30, -40$ mb. After the initial adjustment phase the precipitation is almost independent of $\mathscr{P}$. In the initial adjustment phase, smaller values of $\mathscr{P}$ mean an adjustment towards a moister atmosphere. This initially reduces precipitation for small $\mathscr{P}$. Indeed for faster adjustment times ($\tau = 2$ h is shown), the computed 'precipitation' may initially be negative (Fig. 12). These negative values can easily be suppressed by delaying the convective adjustment until the atmosphere has been sufficiently moistened by the large-scale forcing that the precipitation is positive. (This is done in the global model.) Suppressing 'negative precipitation' has no affect on the subsequent integration after a few hours. For $\mathscr{P} = -40$ mb, the convection scheme is initially intermittent (Fig. 12) as the cloud top selection scheme (which uses a moist adiabat through a low-level $\theta_E$) sees negative buoyancy in the low levels until $\theta_E$ is increased sufficiently by the surface fluxes. This intermittancy does not affect the time-averaged behaviour of the scheme.

The profile of $\mathscr{P}$, given in Table 1, was chosen to give the best overall fit to the vertical structure of relative humidity in the wave (Fig. 4a).
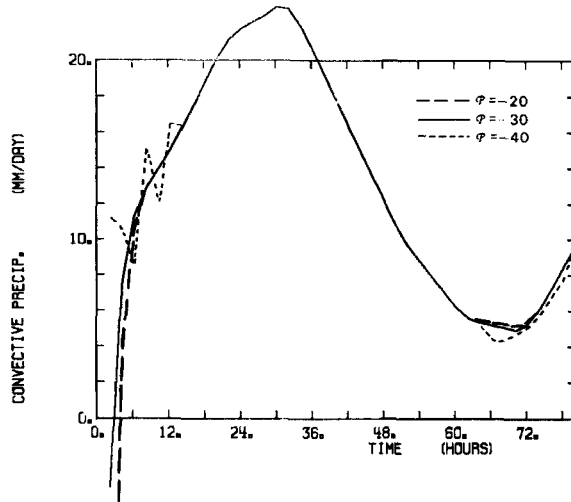
Figure 12.    Model precipitation for $\mathscr{P} = -20$, $-30$ and $-40\,\text{mb}$ (with $\alpha = 1\cdot0$ and $\tau = 2$ hours).

### (d)    Interactive surface fluxes

The tests in sections 2(b) and 2(c) were run with specified surface fluxes added to the lowest model layer (about 982 mb). A version of the model with an extra layer near the surface (and the layer at 150 mb removed) was run with an interactive boundary layer diffusion scheme to compute the surface fluxes. This requires, in addition, the sea surface temperature (fixed at 27 °C) and the surface wind speed. Thompson *et al.* (1979) used mean surface winds and a bulk drag coefficient ($C_E = 1\cdot4\times10^{-3}$ for evaporation) to compute the surface fluxes. These mean winds were reconstructed from the evaporation values in Thompson *et al.*, the difference in $q$ between the surface and the first model level (about 35 m above the surface) and a drag coefficient (appropriate to 35 m) of $C_D = C_E = 1\cdot14\times10^{-3}$. This value of a drag coefficient was computed from the value used by Thompson *et al.* (1979) assuming a logarithmic wind profile:

$$C_D(35) = C_D(10) \left( \frac{\ln(10/Z_o)}{\ln(35/Z_o)} \right)^2$$

with $Z_o = 0\cdot032u_*^2/g$, where $u_*$ is the friction velocity. Figure 13 shows the observed surface fluxes and those computed with the boundary layer scheme, showing that
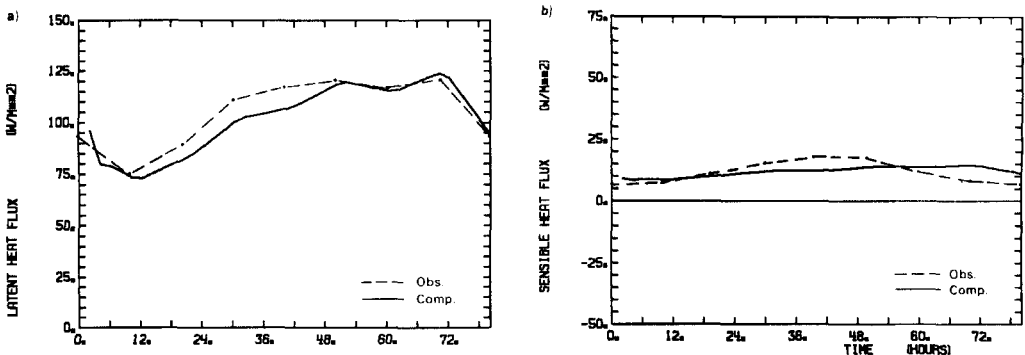


Figure 13.    Comparison of observed (dashed) and computed surface fluxes (solid line) of (a), latent heat and (b), sensible heat with an interactive boundary layer for the GATE wave.
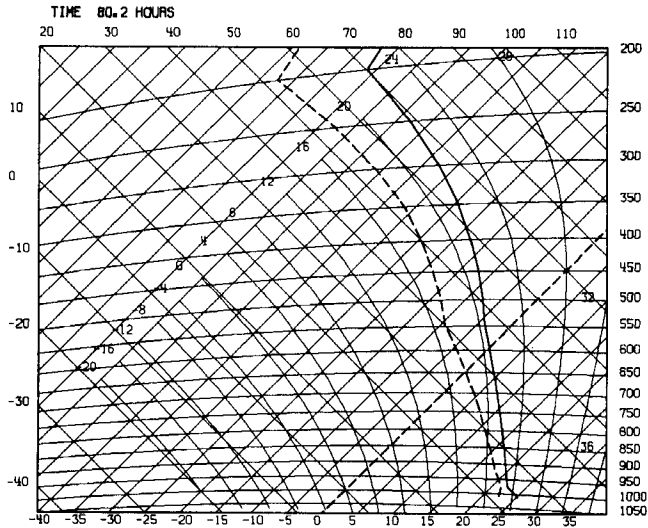
Figure 14. GATE model structure at 80 hours with interactive boundary layer.

the convection scheme and boundary layer diffusion scheme are working together satisfactorily. Figure 14 shows the computed structure at 80 h. Because the convection scheme is not used to adjust the surface layer, the boundary layer diffusion scheme generates a mixed layer between the first two levels.

## 3.  SHALLOW CONVECTION

### (a)  BOMEX data set

The shallow convection adjustment scheme was tested using constant convective and radiative forcing $(Q_1, Q_2, Q_R)$ derived from the budget study of Holland and Rasmusson (1973). Figure 15 shows the large-scale adiabatic terms and radiative cooling used as forcing. The data represent a 5-day mean. A 15-level one-dimensional model was integrated for 72 h to see the response of the convective adjustment to the prescribed large-scale forcing.
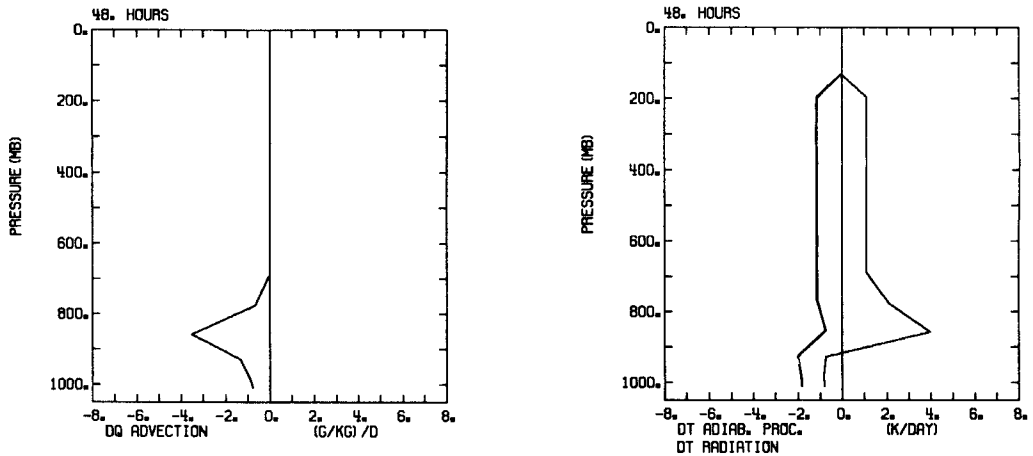


Figure 15.  BOMEX adiabatic and radiative forcing terms.

The model shallow convection scheme finds a cloud top using a moist adiabat through a low-level $\theta_E$, and a mixing line between cloud base and one level above cloud top. Cloud base was kept fixed at $\sigma$ level 14 (about 980 mb). The temperature profile for the convective adjustment has the slope of this mixing line; the moisture profile has constant $\mathcal{P}$. After correcting both temperature and moisture adjustment profiles to satisfy enthalpy and moisture conservation (Eqs. (23), (24) of Betts 1986) the convective adjustment is applied from the cloud base level to cloud top. The boundary layer diffusion scheme computes the fluxes at the surface and below cloud base, and in so doing produces a shallow mixed layer.

Figure 16 shows the structure at 24 h produced by the convection scheme. It is in good agreement with the observed steady state structure although the simulation gives a moister boundary layer. This is probably realistic: further corrections were subsequently made to the BOMEX humidity data which increased the boundary layer specific humidity by 1–2 g kg$^{-1}$ (Rasmusson, personal communication). The simulation is not quite in a steady state. The shallow convection scheme selects 850 mb as the level below cloud top and makes no adjustment at 777 mb, the next model level which is above cloud top. The adiabatic forcing at this level, though small (Fig. 15), is therefore unbalanced and the inversion strengthens with time, although the convection scheme maintains cloud top at the same level. Figure 17 shows the profiles of the parametrized heating and moistening and the boundary layer diffusion terms. It is the convective cooling at 850 mb which is crucial to the maintenance of the trade inversion at this height. In nature it is produced by the evaporation of overshooting cloud tops (Betts 1973): here the parametric scheme, by maintaining the temperature structure against the large-scale subsidence heating, is simulating the process. ECMWF's versions of Kuo's or Arakawa and Schubert's parametrizations do not adequately reproduce this cooling below the trade inversion. The result is that the inversion collapses within 48 h towards the surface, the boundary layer saturates, and the surface evaporation is significantly reduced. An enhanced diffusion scheme (Tiedtke 1983) does succeed in maintaining a more realistic temperature structure up to the inversion, and this is now included in the current operational model.

The surface fluxes are given in Table 2 for different convective adjustment times, $\tau$. The agreement with observation is very good and the variation with the convective adjustment time scale, $\tau$, is small.
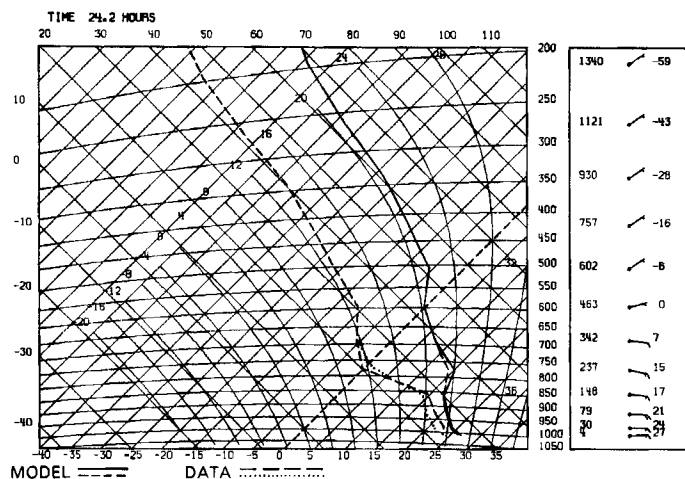


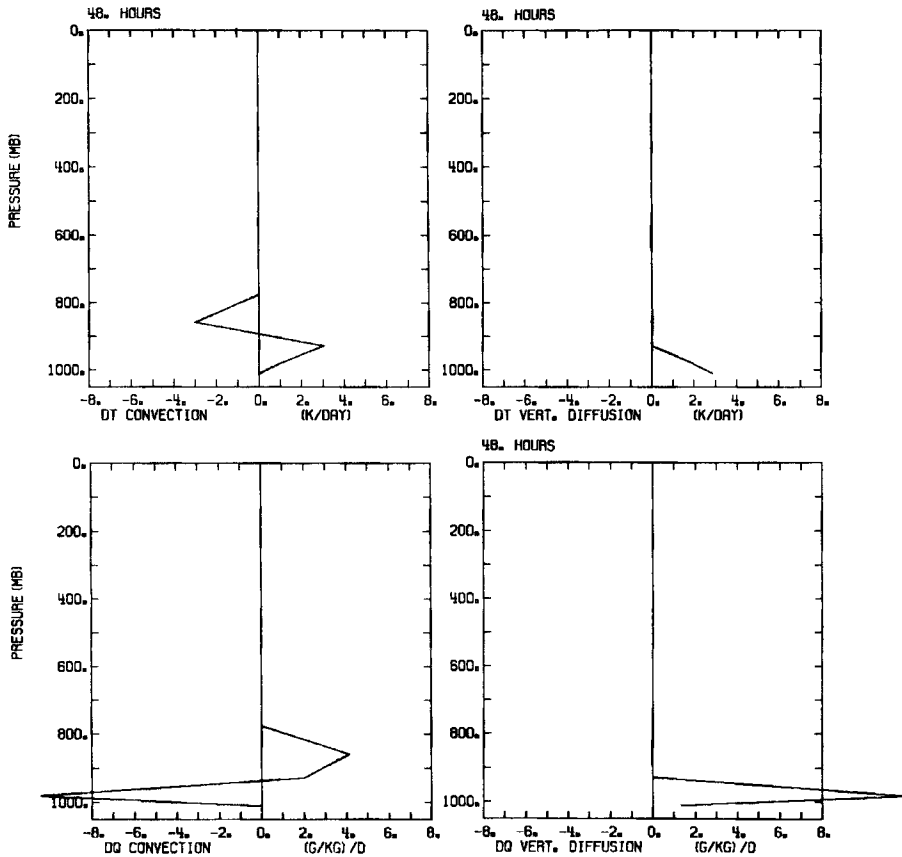Figure 16.  Comparison of observed and model boundary layer structure for BOMEX using convective adjustment scheme.

Figure 17.   Computed BOMEX convective source terms and boundary layer diffusion terms.

## (b)   ATEX data set

The BOMEX tests were repeated for a similar data set derived from the Atlantic trade wind experiment (ATEX) (Augstein et al. 1973; Wagner 1975) with very similar results. Figure 18 shows the comparison of the model and the data (ATEX undisturbed period mean; 7–12 February 1969) at 24 h. The comparison is quite good. In this case, the model temperature profile is more stable than that observed. Figure 8 in part I (Betts 1986) shows that the observed mixing line is somewhat more stable than the cloud layer temperature profile. However, the 'observed' vertical structure may be unrepresentative of horizontal averages because of the special procedure used to generate it (Augstein et al. 1973), which sharpens vertical gradients. In addition, in the model simulation, the

TABLE 2.   COMPARISON OF OBSERVED AND MODEL SURFACE FLUXES FOR BOMEX

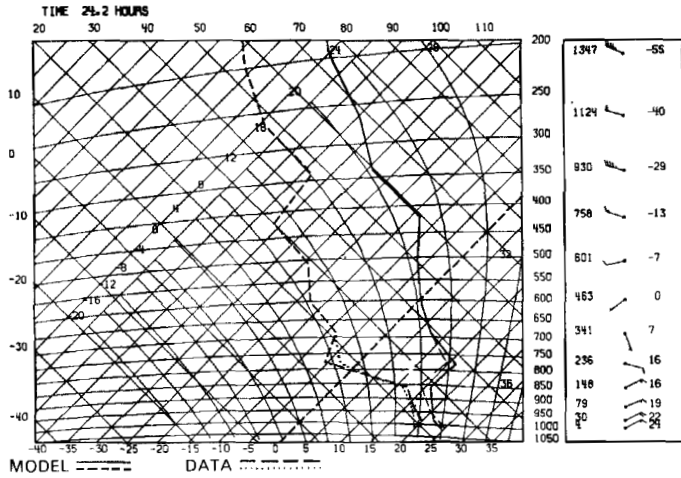| | Model (48 h mean) | | | Observed Holland and Rasmusson (1973) |
|---|---|---|---|---|
| $\tau$ (hours) | 1 | 2 | 3 | |
| Sensible heat flux $(W m^{-2})$ | 17 | 17 | 16 | 15 |
| Latent heat flux $(W m^{-2})$ | 175 | 168 | 161 | 169 |

Figure 18.   As Fig. 16 for ATEX comparison.

mixed layer is too shallow compared with the observations, because of the limited model resolution in the boundary layer.

The model simulation maintains a similar temperature profile for 72 h with an adjustment time scale $\tau = 2$ h; although the inversion strengthens steadily as in the BOMEX case, because the large-scale advective terms are unbalanced slightly at 778 mb. Figure 19 shows that the convective cooling below the inversion is again reproduced. With a faster adjustment time ($\tau = 1$ h) the same inversion height is maintained for 96 h, while for longer $\tau$ ($=3$ h), the inversion starts to fall in height after about 60 h.

Table 3 compares the model surface fluxes with observed values (Krügermeyer 1975). The model values vary little with adjustment time scale, $\tau$, but the computed latent heat fluxes are rather less than the value given by Krügermeyer for the undisturbed ATEX period average (which seems high).
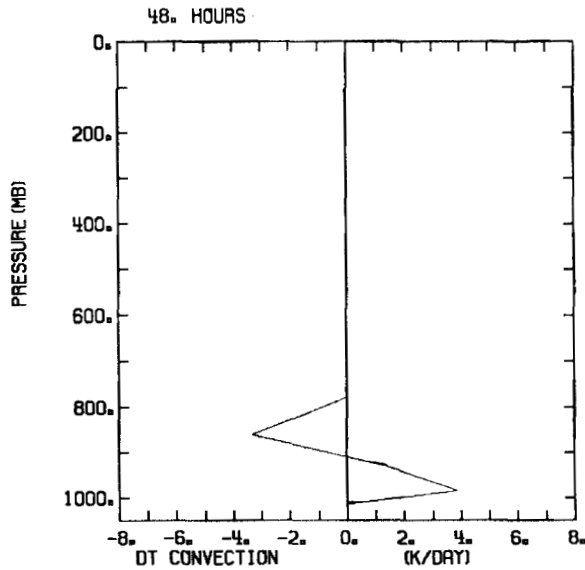


Figure 19.   Computed ATEX convective heat source.

TABLE 3.    COMPARISON OF OBSERVED MODEL SURFACE FLUXES FOR ATEX

|  | Model (48 h mean) | | | Observed Krügermeyer (1975) |
|---|---|---|---|---|
| $\tau$ (hours) | 1 | 2 | 3 | |
| Sensible heat flux (W m$^{-2}$) | 12 | 12 | 13 | 14 |
| Latent heat flux (W m$^{-2}$) | 159 | 154 | 148 | 208 |

## 4.   ARCTIC AIR-MASS TRANSFORMATION

Both shallow and deep convection schemes were tested using an arctic air-mass data set (Økland 1976). This case is discussed in Tiedtke (1977). An initially cold sounding (observed) is advected southward at constant speed over a warmer ocean (with ocean temperatures increasing southward). The surface fluxes are very large and large-scale advective changes and radiation are neglected in comparison. The atmospheric structure after integration for 18 h along this mean southward trajectory is compared with an observed sounding.

In the simulation the shallow convection scheme operates first and the boundary layer deepens, saturates, giving some large-scale precipitation, until the deep convection scheme is activated when cloud top reaches above model level 11 at 765 mb. Convective precipitation replaces large-scale precipitation and the final structure at 18 h compared with the observed structure (a single sounding) is shown in Fig. 20 (using adjustment time scale $\tau = 2$ h). The agreement is reasonable considering large-scale advective terms have been neglected. The observed sounding with a lifting condensation level at 890 mb seems too dry at the surface. The convection top has reached 600 mb by 18 h. Figure 21 shows the sensible and latent heat fluxes at the surface, and the large-scale and convective-scale precipitation.
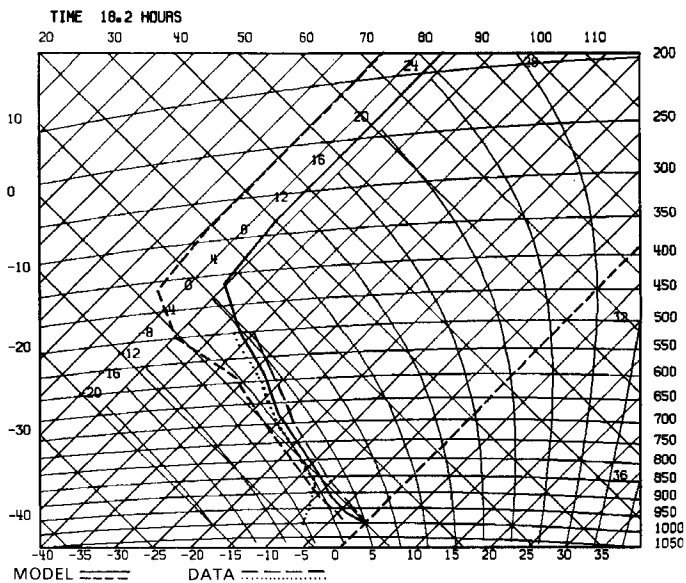


Figure 20.   Comparison of observed and model structure after integration for 18 h along a southerly trajectory for an arctic air-mass transformation.
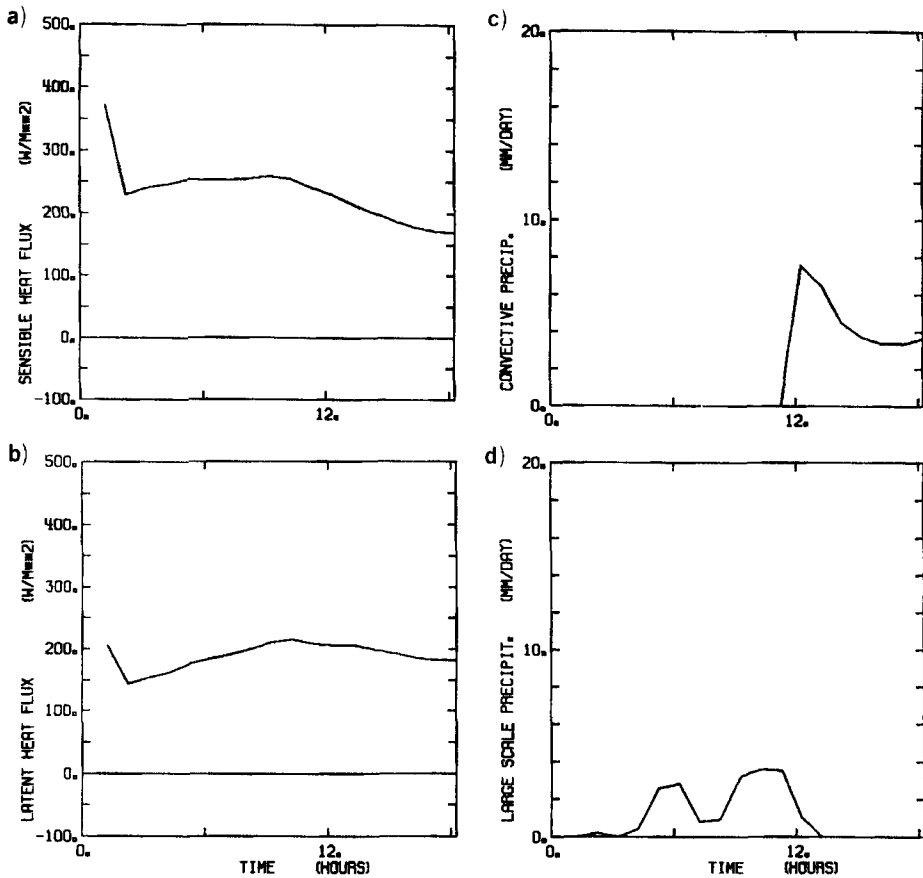
Figure 21.   (a), Sensible and (b), latent heat fluxes; (c), convective and (d), large-scale precipitation; for the arctic air-mass transformation.

The simulation was also repeated specifying a different cloud top level for the transition from shallow non-precipitating to deep convection. Allowing convective precipitation from shallow clouds (tops above model level 12 at 845 mb) reduced the large-scale precipitation, and increased the convective precipitation but did not change the structure at 18 h. On the other hand, if convective precipitation was suppressed until cloud top was higher (above model layer 10 at 678 mb) the atmosphere is saturated with only large-scale precipitation at 18 h (Fig. 22). The 18 h mean surface fluxes, however, change only slightly as the shallow convection transition height is changed. Table 4 summarizes the surface energy fluxes for $\tau = 2$ h.

The interaction of the shallow convective scheme and large-scale precipitation scheme seems satisfactory. Without convective precipitation, the boundary layer saturates with the large surface fluxes. The shallow convection scheme steadily deepens the saturated boundary layer, while the large-scale precipitation scheme removes super-saturation, simulating a deepening stratocumulus layer. Once cloud tops reach a sufficient height, the transition to convective precipitation dries out the boundary layer.

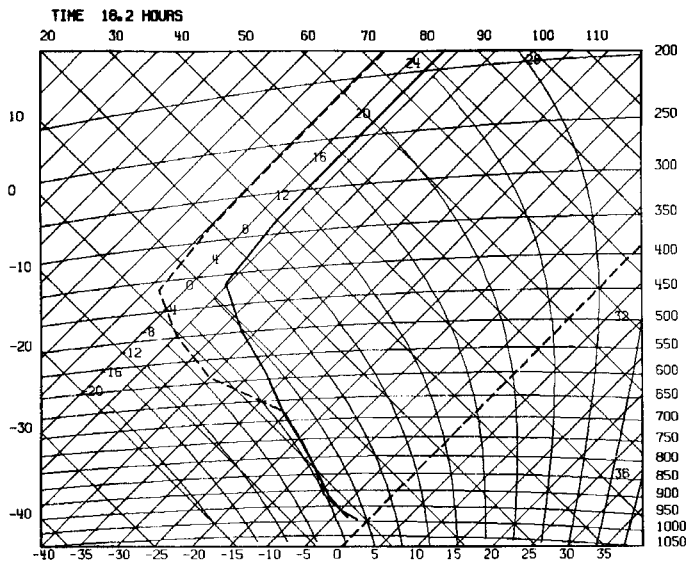These runs were repeated for different adjustment time scales ($\tau = 1$ and 3 h) with similar results.

Figure 22.   Model structure at 18 h with only a shallow convection scheme operating.

## 5. CONCLUDING REMARKS

The single column tests proved of great value in developing the deep and shallow convection components of the convection scheme. The single column GATE wave test differs from the semi-prognostic tests presented by Krishnamurti *et al.* (1980) and Lord (1982) using similar GATE data, since the latter use the cumulus parametrization at each single time. The GATE wave integration presented here integrates forward from an initial structure using given large-scale wave forcing and the convection scheme. Any divergence from the observed wave structure is readily visible. We have tuned the deep convection scheme to reproduce the GATE wave structure by adjusting three parameters (Table 1): the adjustment time, $\tau$; a stability parameter, $\alpha$; and the subsaturation pressure $\mathcal{P}$ (which has been given vertical structure). The scheme smoothly reproduces the GATE wave structure and amplitude, maintaining a vertical thermodynamic structure close to that observed. This was its purpose. In doing so, the convective heat and moisture budgets (Figs. 1(a, b)) predicted by the parametric scheme necessarily agree very closely with those derived from diagnostic budgets, which were used as external forcing. The scheme cannot reproduce the phase of the precipitation exactly, and it seems likely that

TABLE 4.   SURFACE AND PRECIPITATION FLUXES $(W\,m^{-2})$ FOR DIFFERENT
NON-PRECIPITATING BOUNDARY LAYER DEPTHS

| Cloud top limit for no | 12 | 11 | 10 (model level) |
|---|---|---|---|
| convective precipitation | 845 | 765 | 678 (mb) |
| Sensible heat flux | 230 | 234 | 241 |
| Latent heat flux | 191 | 188 | 187 |
| Total heat flux | 421 | 422 | 428 |
| Large-scale precipitation | 12 | 32 | 60 |
| Convective precipitation | 74 | 51 | 0 |
| Total precipitation | 86 | 83 | 60 |

no scheme without subgrid-scale storage of moisture will do this. Subsequent global integrations, which will be presented in a later paper, showed that in a fully interactive model, the convective scheme (when it operated) continued to maintain a vertical temperature and moisture structure typical of deep convection in the tropics. Since the structure parameters were tuned using a GATE data set, it is clear that diagnostic studies from other convective regimes should also be examined. However, as shown in Betts (1986), other deep convective data show to first approximation many similarities in thermodynamic structure with GATE.

The shallow convection tests show that the broad features of shallow cumulus layers capped by a stable layer can be reproduced by the scheme. The limited vertical resolution of cloud top presents some problems though in reproducing diagnostic data closely. The single column tests do not show much sensitivity to the adjustment time, provided it is not more than a few hours. For longer adjustment time scales, the boundary layer depth tends to collapse under the influence of large-scale subsidence. Further study of the time scales involved in maintaining the shallow convective equilibrium structure seems desirable. The vertical structure used in the scheme is based on that found in shallow cumulus boundary layers. More diagnostic studies of the vertical structure within convective boundary layers could lead to further generalization of the scheme. This work is in progress.

Following these single column tests the shallow and deep adjustment schemes were introduced into the ECMWF global forecast model. Extensive tests and studies are still in progress and will be described in a future paper; however, early results are very encouraging and are summarized here briefly.

Comparison of 10-day forecasts using the new convection schemes with the 1984 operational physical parametrization (no shallow convection, Kuo-scheme for deep convection) shows the following marked changes:

There is an increase in surface energy fluxes of 20–30%, and a corresponding increase in convective precipitation. The tropical mean tropospheric temperatures are warmer by about two degrees Kelvin, thus correcting a previously noted global cooling in the ECMWF model (Tiedtke 1982). The strengthened hydrological cycle corresponds to an improved tropical mean flow, with stronger Hadley circulation and trade winds.

It is clear that the shallow convection scheme has a major role in these changes by transporting moisture upward out of the subcloud layer over the tropical oceans and thus enhancing the surface latent heat fluxes. The improvements in the tropics have a generally positive impact on the extratropical flow particularly in the latter part of the forecasts (6–10 days) as might be expected.

REFERENCES

Augstein, H., Riehl, H., Ostopoff, F.    1973    Mass and energy transports in an undisturbed Atlantic trade
    and Wagner, V.                                wind flow. Mon. Wea. Rev., 101, 101–111
Betts, A. K.                             1973    Non-precipitating cumulus convection and its parametrization.
                                                 Quart. J. R. Met. Soc., 99, 178–196

| | 1978 | 'Convection in the tropics'. Pp. 105–132 in *Meteorology over the tropical oceans*. Ed. D. B. Shaw, R. Met. Soc. |
| | 1986 | A new convective adjustment scheme. Part I: Observational and theoretical basis. *Quart. J. R. Met. Soc.*, **112**, 677–691 |
| Cox, S. K. and Griffith, K. T. | 1979 | Estimates of radiative flux divergence during Phase III of the GARP Atlantic Tropical Experiment, Part II: Analysis of Phase III results. *J. Atmos. Sci.*, **36**, 586–601 |
| Frank, W. M. | 1978 | The life-cycles of GATE convective systems. *ibid.*, **35**, 1256–1264 |
| Holland, J. Z. and Rasmusson, E. M. | 1973 | Measurements of the atmospheric mass, energy and momentum budgets over a 500 km square of tropical ocean. *Mon. Wea. Rev.*, **101**, 44–55 |
| Krishnamurti, T. N., Ramanathan, Y., Pau, H. L., Pasch, R. J. and Molinari, J. | 1980 | Cumulus parameterization and rainfall rates. *ibid.*, **108**, 465–477 |
| Krügermeyer, L. | 1975 | 'Vertical transports of momentum, sensible and latent heat from profiles at the tropical Atlantic during ATEX'. Berichte Inst. Radiometeor. und Maritime Meteor., Univ. Hamburg, No. 29 (in German) |
| Lord, S. J. | 1982 | Interaction of a cumulus cloud ensemble with the large-scale environment. Part III: Semi-prognostic test of the Arakawa–Schubert cumulus parameterization. *J. Atmos. Sci.*, **39**, 88–103 |
| Økland, H. | 1976 | 'An example of air-mass transformation in the Arctic and convective disturbances of the windfield'. Report DM-20, Univ. of Stockholm |
| Thompson Jr, R. M., Payne, S. W., Reckel E. E. and Reed, R. J. | 1979 | Structure and properties of synoptic-scale wave disturbances in the intertropical convergence zone of the eastern Atlantic. *J. Atmos. Sci.*, **36**, 53–72 |
| Tiedtke, M. | 1977 | 'Numerical tests of parameterisation schemes for an actual case of transformation of Arctic air'. ECMWF Internal Report No. 10 |
| | 1982 | 'Winter and summer simulations with the ECMWF model'. ECMWF Workshop on Intercomparison of large scale models used for extended range forecasts. 20 June to 2 July 1982 |
| | 1983 | 'The sensitivity of the time-mean large-scale flow to cumulus convection in the ECMWF model'. ECMWF Workshop on Convection in Large-scale Models, 28 Nov.–1 Dec. 1983 |
| Wagner, V. | 1975 | 'Relationships between the tropospheric circulation and energetic processes within the Hadley circulation over the Atlantic Ocean'. Berichte Inst. Radiometeor. und Maritime Meteor. Univ. Hamburg, No. 26 |